Received 14 July 1994; accepted 10 January 1995.

1. Parshall, G. W. *Homogeneous Catalysis* (Wiley Interscience, New York, 1980).
2. Kuntz, E. G. *CHEMTECH* **17,** 570–575 (1987).
3. Yu-Ren Chin Oxo *Alcohols* (Standard Res. Inst. Rep. 21C, SRI International, Menlo Park, California, 1986).
4. Hablot, I., Jenck, J., Casamatta, G. & Delmas, H. *Chem. Engng Sci.* **47,** 2689–2694 (1992).
5. Arhancet, J. P., Davis, M. E., Merola, J. S. & Hanson, B. E. *Nature* **339,** 454–455 (1989).
6. Larpent, C., Debard, R. & Patin, H. *Inorg. Chem.* **26,** 2922–2924 (1987).
7. Waller, F. J. *J. Molec. Catal.* **31,** 123–136 (1985).
8. Borowski, A. F., Cole-Hamilton, D. J. & Wilkinson, G. *Nouv. J. Chim.* **2,** 137–144 (1978).
9. Arhancet, J. P., Davis, M. E., Merola, J. S. & Hanson, B. E. *J. Catal.* **121,** 327–339 (1990).

ACKNOWLEDGEMENTS. We thank G. Samuel for assistance with NMR spectra. This work was supported by the Indo-French Center for Promotion of Advanced Research (Centre Franco-Indien pour la Promotion de la Récherche Avancée), New Delhi.

Modulation of hemispheric sea-ice cover by ENSO events

Per Gloersen

Oceans and Ice Branch, Laboratory for Hydrospheric Research, NASA Goddard Space Flight Center, Greenbelt, Maryland 20771, USA

THE El Niño/Southern Oscillation (ENSO) is a quasiperiodic variation in climate which arises from a complex interaction between the tropical Pacific Ocean and the atmosphere[1]. ENSO events, which occur every two to seven years, are the largest source of interannual variability of temperature and precipitation on a global scale, although their effects are most profound in the tropics[1]. Observations of sea-ice margins have been used to monitor global climate changes on timescales of greater than a decade[2], and there is some evidence for interannual variations in records of sea-ice cover[3]. But short-term changes in sea-ice cover are masked by pronounced seasonal variations, making it difficult to correlate them with specific climate phenomena. Using a multiple-window harmonic analysis technique[4–8], I show here that time series of sea-ice cover from the Arctic and Antarctic contain statistically significant quasi-biennial and quasi-quadrennial periodicities that agree well with variations in the ENSO index. The response of sea ice to these two frequency components varies greatly for different regions.

Quasi-biennial and quasi-quadrennial periodicities attributed to the ENSO appear as significant spectral components in the time series of the length-of-day (LOD) parameter[9–11], as determined from very-long-base interferometer, space geodetic, satellite laser ranging, and Global Positioning Satellite (GPS) data[12]. These spectral components also appear in the atmospheric angular momentum arising from zonally averaged global winds[9,10]. With such clear global effects of ENSO, one might suspect that evidence of the ENSO should also clearly appear in global sea-ice coverage. Weak correlations have been reported earlier in the Bering Sea[13], and the Indian and Pacific oceans[14]. But to date, a clear observation has eluded investigators because of the strong seasonal signal in sea-ice cover as well as localized weather events, which most certainly affect the nearby sea-ice coverage.

The sea-ice cover information discussed here was obtained from an analysis of microwave radiance data collected by the scanning multichannel microwave radiometer (SMMR) operating on board the NASA Nimbus 7 satellite from 26 October 1978 to 20 August 1987[3].

A hint that there may be a Southern Oscillation index/sea ice correlation is shown in Fig. 1*c*, in which a residual obtained by removing the seasonal cycle from a time series of the Arctic sea-ice extents[15] has been smoothed with a running annual average. For comparison, the SOI anomaly (obtained from the NOAA Climate Analysis Center) and the LOD parameter[12], both also smoothed with an annual running average, are shown in Fig. 1*a* and *b*, respectively. As noted earlier[9,10], the SOI signal during 1982–84 (and 1986–87) seems to lead the

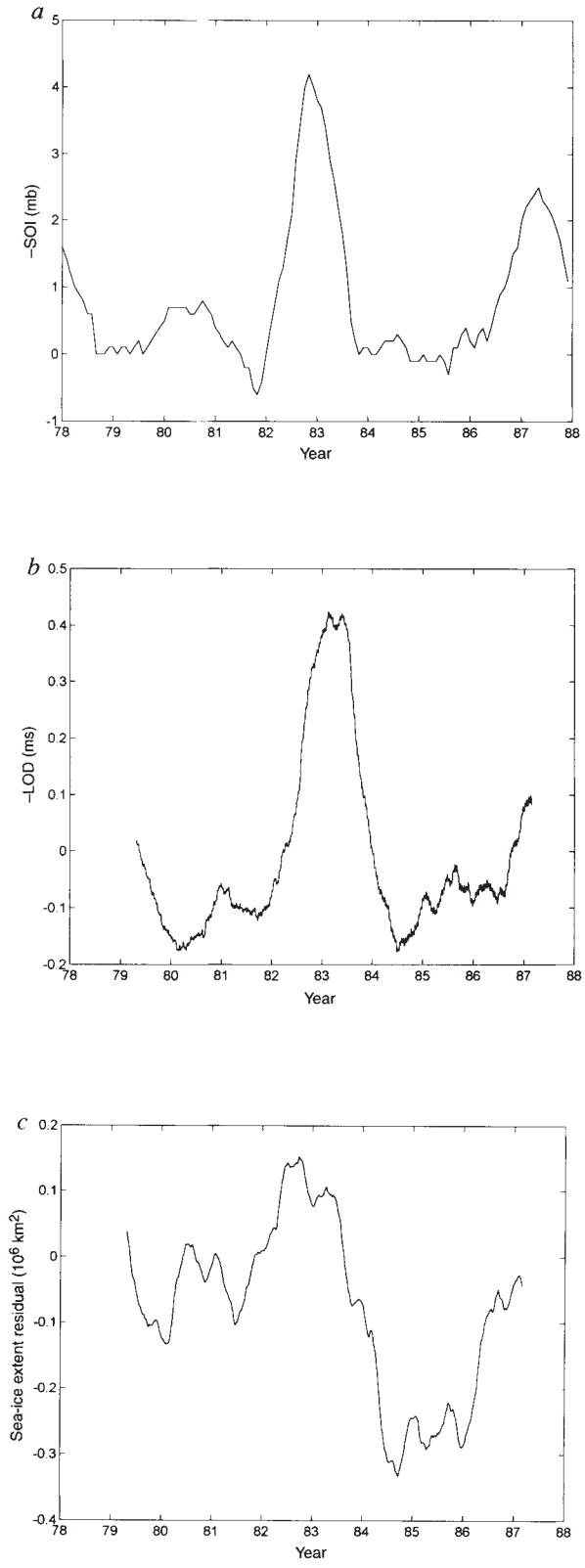

FIG. 1 Running annual averages of: *a*, the negative of the Southern Oscillation Index (SOI) obtained from the NOAA Climate Analysis Center; *b*, the length-of-day (LOD) parameter[12]; *c*, the Arctic sea-ice extent residual[15] (obtained by removing the mean and modelled seasonal cycle from the record of sea-ice extents). The 1983 peak in the negative SOI corresponding to the El Niño event of that year leads that of the LOD by several months. The ice extent has a double peak in 1982–1983, with the second peak approximately in coincidence with the LOD. The first ice-extent peak in 1982 leads both the negative SOI and LOD peaks.

LOD by several months. In the Arctic sea-ice extent residual record, there is a corresponding double peak in the 1982–84 interval.

To clarify comparisons of this sort, I use here a technique developed by others for investigating seismic, atmospheric carbon dioxide, and other time series records[4–8] to examine the unsmoothed time series of ice extents and ice areas (the ice extent less the amount of open water within the ice margin) in a nine-year record obtained from the SMMR[3]. I have also applied the technique to the LOD parameter, which has been suggested as a proxy for the ENSO events[9,10]. This technique permits investigation within a narrow spectral range to exclude interfering events, with the result that the ENSO spectral components are more clearly seen than before in the LOD and for the first time in the sea-ice covers. This technique is summarized in Box 1.

When this procedure is applied to the time series of Arctic ice extents from SMMR[3,15] with values of τ from 1 to 2,920 days, many spectral lines are obtained in which the annual cycle and four of its harmonics predominate. In Fig. 2*a*, I have plotted only the range 400–2,920 days (converted to 1–8 years on the abscissa) in order to emphasize sea-ice oscillations in the range of the ENSO components. A quasi-quadrennial (QQ) component is the strongest line in the spectral distribution of the *F*-statistic with a value of ~4.5, well above the 95% confidence level at the *F*-value of 3.75. There are quasi-triennial (QT) and quasi-biennial (QB) peaks of lesser significance (an *F*-test value of 0.73 represents the 50% confidence level), and some even smaller, but distinct lines at periods of less than two years. The tail of the annual cycle line can be seen at the beginning of the distribution. The spectrum of the Arctic sea-ice area time series[3] in Fig. 2*a* is very similar to that of the Arctic extent, but with generally smaller values of *F*, consistent with the idea that the marginal sea-ice zone might be more sensitive to ENSO forcing than the interior pack. The situation is similar in the Antarctic (Fig. 2*b*), but the *F*-values are generally smaller than in the Arctic, and the QT component is much more prominent.

To permit a direct comparison between SMMR and LOD[12] data, I have performed the above analysis on a subset of the LOD data corresponding in time to the SMMR data. The LOD power spectrum has been presented elsewhere[9,10]; here, I show the spectral distribution of the *F*-test parameter of the LOD in Fig. 1*a* and *b*. There is a close match between the QB and QQ

BOX 1 Multiple-window harmonic analysis scheme

Following procedures described in detail elsewhere[10–14,16], eight different filtered data vectors are produced in the frequency domain by the Fourier transformations:

$$y_k(\tau) = \sum_{t=1}^{3,224} V_k(t) y(t)\, e^{-2\pi i t/\gamma} \quad k = 1, 2, \ldots, 8 \qquad (1)$$

where $V_k(t)$ is a data window of bandwidth $2W$ (with W chosen to be $4/N$, N being the number of observations) computed by taking a singular value decomposition of the sinc matrix[4], and $1/\tau$ is the central frequency of the spectral band. **y** is the data vector. The sum over time t is taken on six-day intervals for the sea-ice data, to match the revisit time of the SMMR, and on one-day intervals for the LOD data. The coefficients of the model solution are obtained from the weighted sum of the eight differently-windowed and transformed data vectors, $\mathbf{y_k}$:

$$a(\tau) = \sum_{k=1}^{8} \frac{y_k(\tau) V_{0k}}{\sum_{k=1}^{8} V_{0k}^2} \qquad (2)$$

where V_{0k} is a normalizing factor obtained by summing the columns of $V_k(t)$.

The unexplained variance (in the frequency domain, and within the spectral bandwidth, $2W$) is then obtained by summing the squares of the differences between each of the eight windowed and transformed data vectors and the weighted coefficients of the model solution:

$$e^2(\tau) = \sum_{k=1}^{8} \{[y_k(\tau) - a(\tau)V_{0k}][y_k(\tau) - a(\tau)V_{0k}]^*\} \qquad (3)$$

where * indicates the complex conjugate.

To obtain a test of statistical significance for the spectral lines that result from the model solution amplitudes, $a(\tau)$, I have used an *F*-test statistic, which is written in terms of the ratio of the explained to unexplained variance within the bandwidth, $\pm W$:

$$F(\tau) = \{(n-1)[a(\tau)a^*(\tau)] \sum_{k=1}^{8} V_{0k}^2\} / e^2(\tau) \qquad (4)$$

In the present case, $n = 8$, the number of independent samples of the data vector in the frequency domain. The random variable *F* has 2 and $2n-2$ degrees of freedom if the data are normally distributed.

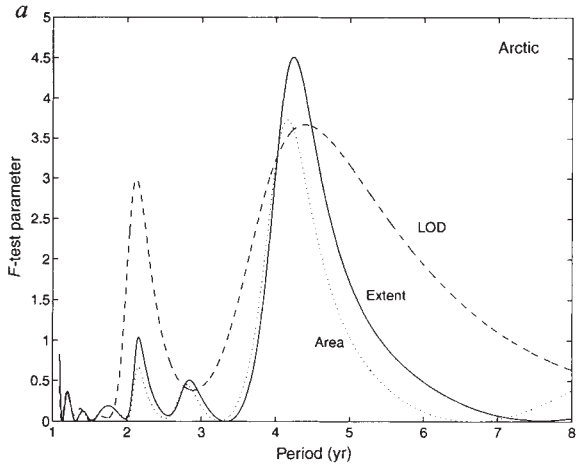

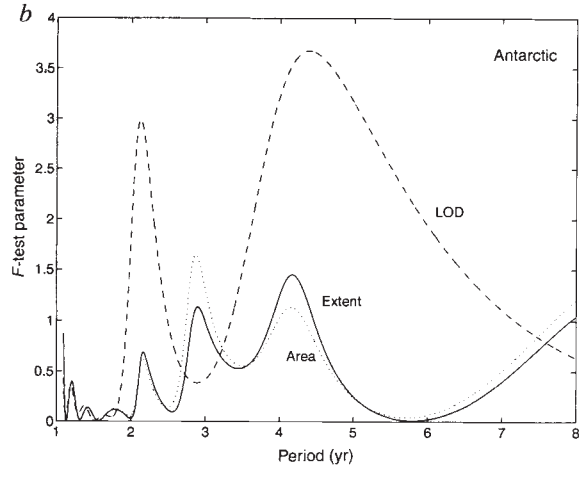

FIG. 2 Spectral distribution of the *F*-test periodicity in the nine-year time series of sea-ice area and extent in the Arctic (*a*) and the Antarctic (*b*). The LOD spectrum is superimposed for comparison. In the Arctic, the quasi-quadrennial (QQ) peak, at about 4.2 years, for the ice extent has a confidence level of 97%; those of the ice area and LOD, 94.5%. The strong quasi-biennial (QB) peak in the LOD shows up in the sea-ice area and extent with lower confidence levels, 60% or less. The *F*-test values were obtained by first filtering the data with multiple-window tapers devised with prolate spheroid functions[16] and then performing a discrete Fourier transform on the filtered data to obtain the complex coefficients of the model fit to the data. The *F*-test is the ratio of the explained variance (modelled data) to the unexplained variance (observed data minus the modelled data) within the bandwidth, $\pm W$, ~1/806 d^{-1}.

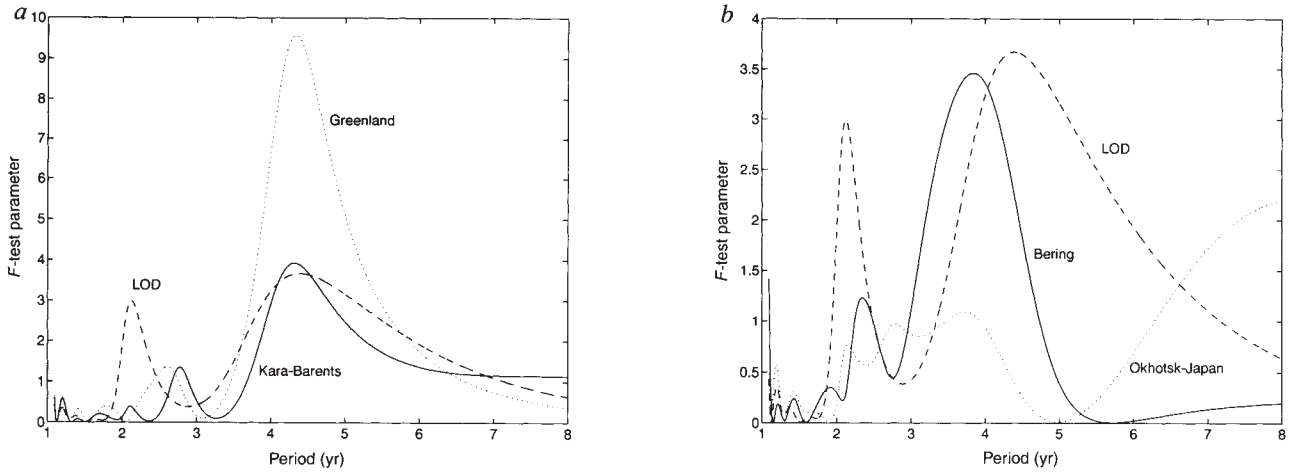

FIG. 3 Same as Fig. 2, except for the sea-ice area only in: *a*, the Greenland and Kara–Barents regions; *b*, the Bering and Okhotsk–Japan regions[3]. The confidence level of the QQ component in the Kara–Barents region is ~95%; in the Greenland Sea, well above 99%. The QB and QQ components in the Bering and Okhotsk–Japan regions are shifted to higher and lower periods, respectively, than those of the LOD.

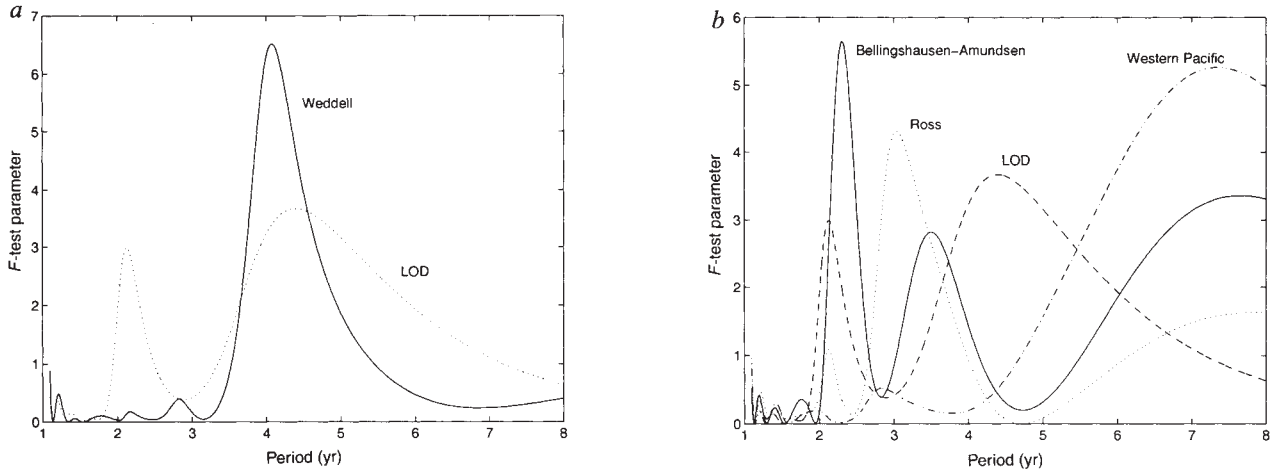

FIG. 4 Same as Fig. 2, except for the sea-ice area only; *a*, in the Weddell Sea sector[3]; *b*, in the Bellingshausen–Amundsen, Ross and Western Pacific sectors[3]. In the Weddell Sea sector, the QQ component predominates, whereas in the Bellingshausen–Amundsen Seas sector, the QB component is dominant. There is a strong quasi-triennial (QT) component in both the Bellingshausen–Amundsen and Ross Sea sectors. There are no substantial QB, QT, or QQ components in the Western Pacific sector, nor in the Indian Ocean sector[3] (not shown).

components of the LOD and those of the Arctic and the Antarctic. The QT component in the Arctic and Antarctic is missing in the LOD spectrum because the LOD time series used here is on exactly one-day intervals. The QT component appears to be an alias frequency resulting from the beating of the SMMR revisit frequency against the S_1 (and/or S_2) oceanic/atmospheric tidal frequency.

Pursuing the idea of greater ENSO sensitivity in the marginal sea-ice zones, I have selected for similar analysis the Arctic regions, defined elsewhere[3], that include some of the perimeter seas. The most prominent indication of the QQ component, about twice the *F*-value of that in the Arctic ice extent (Fig. 2*a*), occurs in the time series of the Greenland Sea ice areas (Fig. 3*a*), where also the QB and QT components are not as distinct. The QQ component in the Kara–Barents region (Fig. 3*a*) is comparable to that of the Arctic extent, and the QT component is more distinct. In the Bering region (Fig. 3*b*), the QQ and QT components appear to have shorter periods than the Arctic sum by about half a year. In the Okhotsk–Japan region, the QQ, QT and QB components run together and are all below the 70% confidence level (Fig. 3*b*).

Turning to the Antarctic, the Weddell Sea sector[3] shows the QQ component as the only significant peak (Fig. 4*a*). The QB component is the strongest in the Bellingshausen–Amundsen sea sector[3] (Fig. 4*b*). The Ross Sea sector[3] shows a strong QT peak and a weaker QB peak.

It is clear that variations in the areal coverage of sea ice on global, hemispheric and regional bases contain periodicities of quasi-biennial and quasi-quadrennial components, very similar to the variations in the length-of-day, El Niño–Southern Oscillation index and atmospheric angular momentum parameters[9,10]. The average response to these two components is more significant in the Arctic than in the Antarctic. However, the regional responses to these two components vary greatly. The QQ oscillation is most significant in the Greenland Sea region and almost as significant in the Weddell Sea, whereas the QB com-

ponent is most significant in the Bellingshausen–Amundsen Sea sector. □

Received 11 August; accepted 8 December 1994.

1. Philander, S. G. H. *El Niño, La Niña and the Southern Oscillation* (Academic, New York, 1990).
2. Lamb, H. H. *Climate: Past, Present, and Future* (Methuen, London, 1972).
3. Gloersen, P., Campbell, W. J., Cavalieri, D. J., Comiso, J. C., Parkinson, C. L. & Zwally, H. J. *Arctic and Antarctic Sea Ice, 1978–1987: Satellite Passive-Microwave Observations and Analysis* (SP-511, NASA, Washington DC, 1992).
4. Lindberg, C. R. thesis, Univ. California, San Diego (1986).
5. Park, J., Lindberg, C. R. & Vernon, F. L. *J. geophys. Res.* **92,** 12675–12684 (1987).
6. Park, J., Lindberg, C. R. & Thomson, D. *J. Geophys. J. R. astr. Soc.* **91,** 755–794 (1987).
7. Lindberg, C. R. & Park, *J. Geophys. J. R. astr. Soc.* **91,** 795–836 (1987).
8. Kuo, C., Lindberg, C. R. & Thomson, D. J. *Nature* **343,** 709–714 (1990).
9. Dickey, J. O., Marcus, S. L. & Hide, R. *Nature* **357,** 484–488 (1992).
10. Dickey, J. O., Marcus, S. L., Eubanks, T. M. & Hide, R. *Interactions Between Global Climate Systems, The Legacy of Hann* 141–155 (Geophys. Monogr. 75, Am. Geophys. Union, Washington DC, 1993).
11. Chao, B. F. *Science* **243,** 923–924 (1989).
12. Gross, R. S. & Steppe, J. A. *A Combination of Earth Orientation Data: SPACE93* (Observetoire de Paris, 1993).
13. Niebauer, H. J. *J. geophys. Res.* **93,** 5051–5068 (1988).
14. Simmonds, I. & Jacka, T. H. *J. Clim.* (in the press).
15. Gloersen, P. & Campbell, W. J. *Nature* **352,** 33–36 (1991).
16. Thomson, D. J. *Proc. IEEE* **70,** 1055–1095 (1982).

ACKNOWLEDGEMENTS. I thank E. Mollo-Christensen, D. J. Cavalieri, S. Hakkinen and C. J. Koblinsy for helpful suggestions. This work was sponsored by the Science Division of the Office of Mission to Planet Earth at NASA Headquarters.

Climate-related variations in denitrification in the Arabian Sea from sediment $^{15}N/^{14}N$ ratios

Mark A. Altabet*, Roger Francois*, David W. Murray† & Warren L. Prell†

* Marine Chemistry and Geochemistry Department, Woods Hole Oceanographic Institution, Woods Hole, Massachusetts 02543, USA
† Department of Geological Sciences, Brown University, Box 1846, Providence, Rhode Island 02912, USA

DENITRIFICATION—the process by which nitrate is reduced to gaseous nitrogen species (usually N_2 or N_2O)—is the dominant mechanism for removal of fixed nitrogen from the biosphere. In the oceans, denitrification is mediated by bacteria in suboxic environments and, by controlling the supply of fixed nitrogen, is an important limiting factor for marine productivity[1–3]. Denitrification produces substantial ^{15}N enrichment in subsurface nitrate[4–6], which is reflected in the isotopic composition of sinking particulate nitrogen[7]; sediment $^{15}N/^{14}N$ ratios in regions with suboxic water columns may therefore provide a record of past changes in denitrification intensity. Here we report nitrogen isotope data for sediment cores from three sites in the Arabian Sea. At all three sites we find large, near-synchronous downcore variations in $^{15}N/^{14}N$, which are best explained by regional changes in the isotopic composition of subsurface nitrate, and hence denitrification. Moreover, these variations are synchronous with Milankovitch cycles, thereby establishing a link with climate. We argue that these large, climate-linked variations, in a region that contributes significantly to global marine denitrification, are likely to have perturbed marine biogeochemical cycles during the Late Quaternary period.

The $^{15}N/^{14}N$ ratio of particulate organic matter sinking out of the surface ocean is principally a function of the $\delta^{15}N$ (in ‰ relative to atmospheric N_2: see Fig. 2 legend) of source nitrate (NO_3^-, transported vertically from subsurface waters) and isotopic fractionation occurring during partial utilization of this nutrient by phytoplankton[8,9]. Recent results have shown this surface-generated isotopic signal to be subsequently recorded in deep-sea sediment[10]. In the equatorial Pacific and the Southern Ocean, large latitudinal gradients in $\delta^{15}N$ for both near-surface ocean particulate organic matter and core-top sediments are inversely correlated with surface $[NO_3^-]$. In these regions, variations in $\delta^{15}N$ are driven by variations in nutrient utilization because the $\delta^{15}N$ of subsurface NO_3^- is fairly constant throughout most of the ocean[6]. But in oceanic regions with suboxic subsurface waters (that is, strong oxygen-minimum zones), denitrification also produces substantial enrichment in ^{15}N for the residual NO_3^- (refs 5, 6) which extends regionally[6] as a result of horizontal advection and mixing. By producing regional increases in the $\delta^{15}N$ of subsurface NO_3^-, water-column denitrification strongly influences the $\delta^{15}N$ of sinking particulate organic matter and sediments in these domains[7,11].

We have examined sediment cores at three sites in the Arabian Sea to isolate past variations in these effects (Fig. 1). Summer monsoon winds produce upwelling along the Oman coast out to ~350 km of shore. At this time when productivity and downward particle fluxes are high[12,13], the corresponding northwest to southeast gradient in surface nutrients[14] may be expected to produce spatial variations in the $\delta^{15}N$ of near-surface particulate organic matter. Near-core-top sediments do show a 1‰ increase from the margin outwards to the Owen ridge (350 km offshore; Fig. 2). The Owen ridge (RC27-61) and nearshore Oman margin sites (ODP site 723, hole B and RC27-24) are at the edge and well within the upwelling system, respectively. Past changes in the gradient in $\delta^{15}N$ between them could reflect changes in the

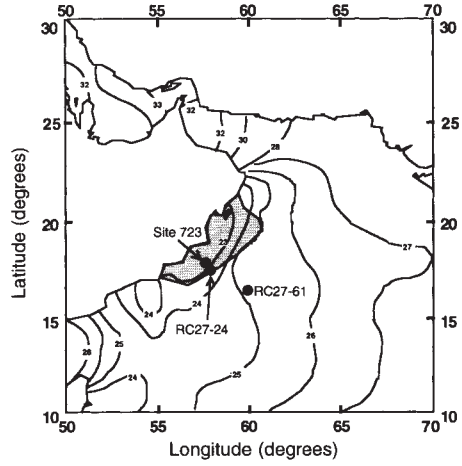

FIG. 1 Core locations in the northwest Arabian Sea. RC27-24 (17° 43.1′ N, 57° 49.2′ E; 1,416 m depth) and ODP site 723 (18° 3.1′ N, 57° 36.6′ E; 808 m depth) are from the Oman margin. RC27-61 (16° 39.5′ N, 59° 31.4′ E) is located 350 km offshore at 1,893 m depth. Contours of summer sea surface temperature show the gradient in monsoon-driven upwelling intensity[36]. The shaded area shows the region of high-nutrient surface waters ($[PO_4^{3-}] > 1$ μM) associated with upwelling[14]. Suboxic water between 100 and 1,000 m depth is present throughout most of this region, including over our core sites. Comparing results for the two cores in the Oman margin shows that depositional environment has little effect on sedimentary $\delta^{15}N$ in this region. Site 723 at 808 m depth is overlain by the oxygen-minimum zone; core RC27-24, 24 km to the southeast at 1,416 m water depth, is overlain by oxic water. Despite large differences between site 723 and RC27-24 in particulate nitrogen content (for example, 1% and 0.45%, respectively, at core top; the sedimentary nitrogen accumulation rates show similar differences), the downcore $\delta^{15}N$ variations are very similar for these two sites (Fig. 2). For the Late Holocene, values are indistinguishable. Considering that these sites are sufficiently close to receive the same input from near-surface waters, the differences in %N and N accumulation rate are probably related to contrasts in nitrogen preservation and/or along-bottom transport or trapping of sediment. In either case, these results indicate that possible past changes in depositional environment are unlikely to have significantly influenced the $\delta^{15}N$ recorded in this region.